THE BALTIC JOURNAL
OF ROAD AND BRIDGE ENGINEERING
2025/20(4)

ISSN 1822-427X/eISSN 1822-4288
2025 Volume 20 Issue 4: 1–29
https://doi.org/10.7250/bjrbe.2025-20.663

OUT-OF-PLANE BUCKLING MECHANISM AND ENHANCING METHOD OF STIFF SKELETON ARCH BRIDGE WHEN WRAPPING SURROUNDING CONCRETE

TAO WANG[1, *], LINQI ZHOU[2], HAO CHEN[2]

[1]*Highway Institute, Henan College of Transportation, Zhengzhou, China*

[2]*School of Civil Engineering, Chongqing Jiaotong University, Chongqing, China*

Received 28 November 2024; accepted 26 August 2025

Abstract. This study investigates the stability of skeleton-reinforced concrete arch bridges during the concrete encasement process, employing a homogeneous generalized yield functions for extreme buckling load determination in nonlinear finite element analysis. Through an analysis of the stability of a stiff skeleton arch bridge with a 600 m span during the concrete wrapping stage, this study delves into and elucidates the mechanism by which the transverse brace enhances the out-of-plane stability capacity of the skeleton arch ribs. Additionally, a method for improving stability by controlling the lateral rotation angle of arch ribs is proposed. The results indicate that the lateral deflection angle of arch ribs serves as a crucial metric for assessing the out-of-plane stability of arch bridges. Transverse braces effectively coordinate and constrain the lateral deflections of two isolated arch ribs through their bending stiffness along the tangential direction of the arch axis. Notably, transverse braces within the range of L/8 to 3L/8 make the most substantial contribution to the lateral stiffness of arch ribs. Consequently, wrapping surrounding concrete on transverse braces within the L/8 to 3L/8 range proves advantageous for enhancing the stability of a stiff

* Corresponding author. E-mail: 147625027@qq.com

Tao WANG (ORCID ID 0009-0008-2301-0208)

skeleton arch bridge under construction. Specifically, it is recommended to pour surrounding concrete on transverse braces at L/4 before the closure of the bottom plate's concrete ring. After the ring of bottom plate's concrete is closed, a symmetrical pouring of surrounding concrete on transverse braces from L/4 to the arch spring and vault is proposed.

Keywords: concrete arch bridge, double-nonlinear, out-of-plane instability, stiff skeleton, transverse brace.

Introduction

The stiff skeleton method was first proposed by Czech engineer Joseph Melan in 1898. This non-bracket construction scheme is typically known as the stiff skeleton construction method, in which a concrete-filled steel tube (CFST) arch bridge must be built in advance to support the concrete formwork for warping the surrounding concrete. In the 1990s, China began to apply the concrete-filled steel tubular structure to the arch bridge, and successfully built the Wanzhou Yangtze River Bridge, a concrete arch bridge with a span of 420 m. The development of construction techniques for a stiff skeleton concrete arch bridge significantly promotes the construction of arch bridges in mountainous areas of China (Zheng and Wang, 2017). According to incomplete statistics, 21 concrete arch bridges spanning over 100 m have been built by a stiff skeleton method in the last twenty years (Zhao et al., 2021).

In the late 1980s, Japan proposed the construction method of combined arch support, pipe support, or combined steel pipe support (concrete) pouring, which is called the combined arch frame method, pipe arch frame method, or combined steel pipe arch frame method. It adds a step of pouring concrete into the box on the basis of the general steel box arch frame, which can enhance the rigidity of the arch frame.

The stiff skeleton concrete arch bridge is constructed using pre-hoisted precast concrete arch ribs as the framework. In the construction stage of a stiff skeleton concrete arch bridge, the surrounding concrete on stiff skeletons is typically cast-in-place on multiple working platforms, ring by ring (Shao et al., 2017), as shown in Figures 1 and 2. Before the longitudinal closure of each arch ring, the concrete on stiff skeletons is a number of discrete plates, which fail to form an integral arch structure to bear the self-weight together with the closed arch ring. Only after each ring of concrete is closed will it bear the weight of the subsequent poured concrete together with the stiff skeleton. Therefore, the instantaneous stiffness of arch is weakest when each arch ring is about to close, as the poured segments without closure fail to form an integrated arch structure to provide effective stiffness. With the increase in the span of stiff skeleton arch bridges, the instability risk in the process of wrapping the surrounding concrete on stiff skeletons becomes more and more serious.

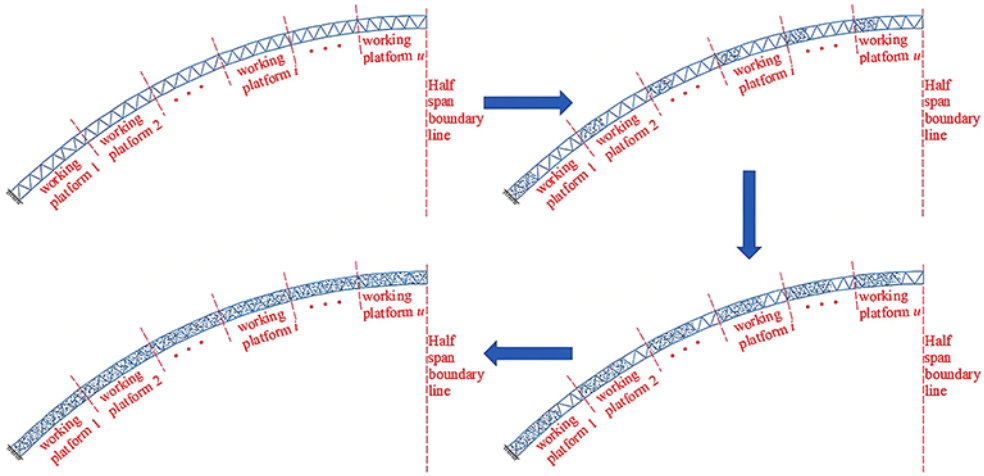

Figure 1. Wrapping scheme of the surrounding concrete on multiple working platforms placed on a stiffened skeleton

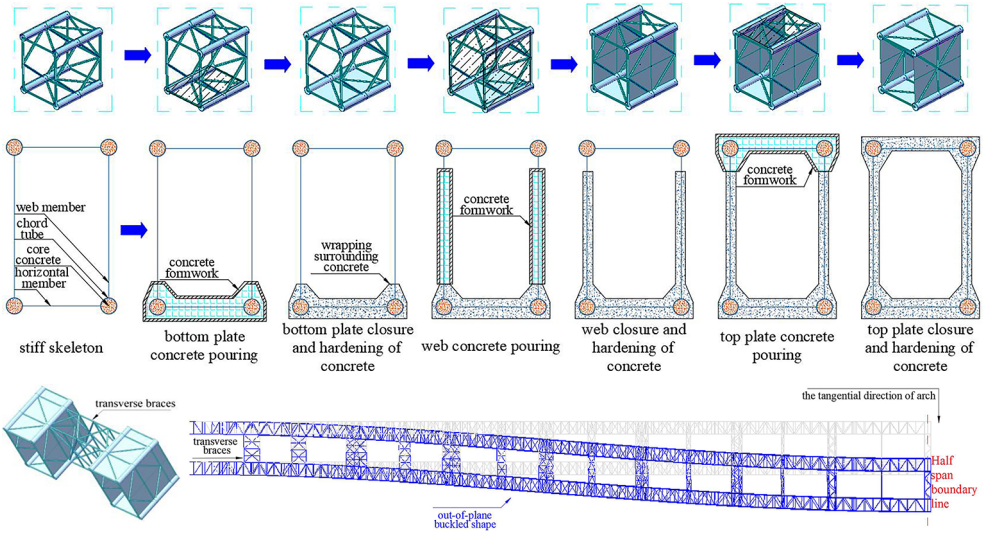

Figure 2. Diagram of ring-by-ring wrapping scheme of the surrounding concrete on a stiffened skeleton and out-of-plane buckled shape of arch

In the 20th century, many scholars (Godden, 1954; Stüssi, 1943; Waestlund, 1960) discussed the out-of-plane buckling problem of arch structures. Analytical solutions of buckling loads corresponding to circular arches, curved rods with identical

cross-sections were proposed. Later, a finite element method gained much attention to study the critical load of out-of-plane buckling of arch structures (Mackenzie et al., 2000; Tong et al., 2022; Yang et al., 2015), as analytical methods cannot deal with complex arch structures and cannot take into account geometric and material nonlinearity in buckling analysis. Several researchers (Geng et al., 2018; Lu et al., 2022; Luo et al., 2015; Pi et al., 2011) studied the long-term structural behaviours and stability performance of CFST arch bridges, and declared that the long-term increment in deflection and internal force predicted by nonlinear analysis was much more significant than that predicted by linear analysis. Thus, it is essential to conduct nonlinear analysis to evaluate the stability of arch bridges under long-term loads. Besides, the nonlinear analysis of stiff skeleton arch bridges by FEM showed that the reduction of structural stability by the coupling effect of geometric and material nonlinearity would be much greater than that considering a single nonlinearity (Chen et al., 2019; Cheng et al., 2002; Rakici and Menkulasi, 2021; Xie et al., 2021). Therefore, the influence of geometric and material nonlinearity must be considered simultaneously when evaluating the stability performance of stiff skeleton arch bridges. However, it is time-consuming and laborious to seek for the ultimate stability capacity by nonlinear buckling analysis. Thus, it is worthy to develop a sufficient method to evaluate the nonlinear stability capacity of stiff skeleton arch at every stage of surrounding concrete pouring, so that the pouring procedures of surrounding concrete can be optimised.

At the same time, the way of improving the out-of-plane stability of rib arch bridges has attracted extensive attention. Currently, the main idea for improving the out-of-plane stability of arch bridges is to optimise and adjust the structural configuration and arrangement of transverse braces (Xu et al., 2007). It is well accepted that the transverse brace, especially its bending stiffness along the tangential direction of arch (Ji and Shi, 2011; Liu et al., 2014), greatly contributes to the lateral bending stiffness of double-rib arch bridges. Therefore, it is more efficient to enhance the out-of-plane stability capacity of double-rib arches by increasing transverse braces' bending stiffness along the tangential direction of arch rather than the stiffness along the tangential direction of arch. In addition, studies (Li et al., 2008; Song and Chen, 2012; Dong et al., 2020) found that the transverse brace in X-shape was the most efficient structural configuration to enhance the out-of-plane stability capacity of double-rib arches, followed by K-shape, star shape, L-shape, and I-shape. This conclusion also indicates that the increase in bending stiffness of the transverse brace along the tangential direction of the arch rib may improve the out-of-plane stability of double-rib arches. To find out the influence of transverse braces' location on the out-of-plane stability of the arch ribs, Gu (2011) studied the influence of the location of three, five, and seven transverse braces on the out-of-plane buckling load of a double-rib arch. Wang et al. (2018) studied the variation in the elastic stability coefficient of a stiff skeleton arch bridge when pouring surrounding

concrete on different transverse braces. Zheng et al. (2012) examined the influence of temporary transverse braces on the out-of-plane elastic stability of arch rib during construction. Chen et al. (2010) analysed the influence of transverse brace location on geometric-nonlinear stability of arch rib. They claimed that arranging transverse braces in the range of arch foot to one-quarter span point might greatly enhance the out-of-plane stability of arch ribs, while additional transverse braces at the arch crown were not so noticeable.

In terms of research methodology, nonlinear finite element analysis has emerged as the predominant approach to assessing the stability of arch bridges. This method takes into account geometric nonlinearity, material nonlinearity, and initial imperfections, thereby enabling a more precise prediction of the bridges' ultimate load-bearing capacity. For instance, in 2023, Červenka and colleagues introduced a three-dimensional concrete analysis method that integrates fracture and plasticity material models. This method has been widely adopted in engineering practice.

Although the reasonable structure of transverse braces and their arrangement schemes in separated-rib arch bridges have been reported, current studies on the out-of-plane stability of separated-rib arches are mostly case studies. The enhancing mechanism of the transverse brace to the out-of-plane stability of arch ribs has not been clarified. Additionally, there is no quantitative index to evaluate the enhancement of out-of-plane stability performance of arch ribs by transverse braces. As the pouring procedures of transverse brace concrete may affect the lateral stability of arch ribs, it is worthwhile to explore a quantitative method to evaluate the out-of-plane stability of stiff skeleton arch bridges when wrapping surrounding concrete.

A qualitative method to evaluate the out-of-plane stability of stiff skeleton arch bridges is proposed in this study. A stiff skeleton arch bridge with a span of 600 m is taken as an example to discuss the variation in stability performance during wrapping the surrounding concrete on skeletons, to study the influence of pouring procedures of surrounding concrete on transverse braces on the elastic stability of the main arch. Furthermore, a method to improve the out-of-plane stability of arch ribs based on the control of the lateral rotation angle of the arch rib is proposed and verified.

The out-of-plane stability of separated-rib arch bridges has garnered significant attention in civil engineering. While numerous studies have documented the reasonable structure of transverse braces and their arrangement schemes in these bridges, the existing research predominantly consists of case studies. A comprehensive understanding of the enhancing mechanism of transverse braces on the out-of-plane stability of arch ribs remains elusive. This knowledge gap is further compounded by the lack of a quantitative index to assess the enhancement of out-of-plane stability performance of arch ribs achieved through the use of transverse braces.

Moreover, the pouring procedures of transverse brace concrete can have a substantial impact on the lateral stability of arch ribs. Given this critical factor, it is imperative to develop a quantitative method to evaluate the out-of-plane stability of stiff skeleton arch bridges when wrapping surrounding concrete.

In this study, we aim to address these knowledge gaps and propose a qualitative method to evaluate the out-of-plane stability of stiff skeleton arch bridges. Taking a stiff skeleton arch bridge with a span of 600 m as a case study, we investigate the variation in stability performance during the process of wrapping the surrounding concrete on the skeletons. This analysis allows us to examine the influence of the pouring procedures of the surrounding concrete on transverse braces on the elastic stability of the main arch. Furthermore, we introduce a novel method to improve the out-of-plane stability of arch ribs based on the control of the lateral rotation angle of the arch rib. This method is not only proposed but also rigorously verified through our research.

1. An efficient qualitative method for evaluating the ultimate buckling capacity of stiff skeleton arches during casting surrounding concrete

1.1. Accurate evaluation by nonlinear buckling analysis

The elastic buckling analysis of an arch structure is essentially an eigenvalue problem. Although elastic buckling analysis is efficient, there is a significant deviation between the elastic buckling load and the real buckling load without accounting for the nonlinearity and initial defects. In nonlinear buckling analysis, geometric-nonlinearity, material-nonlinearity, and initial defects can all be taken into consideration. The incremental iteration method is generally used to solve the equilibrium. The extreme point in this load-deflection curve is regarded as the ultimate bearing capacity of the actual structure.

The ratio of ultimate buckling load to the service load under normal state is usually referred to as the nonlinear stability safety factor K as shown in Equation (1):

$$K=\frac{P_{\mathrm{cr}}}{\left(P_{\mathrm{g}}+P_{\mathrm{q}}\right)}, \tag{1}$$

where P_{cr} is the ultimate buckling load; P_{g} and P_{q} are dead load and live load, respectively.

A stiff skeleton arch bridge is usually composed of numerous components in space, and its spatial mechanical behaviour and nonlinear characteristics are

noticeable. Therefore, it is difficult to achieve an analytical solution of critical buckling loads from Equation (1) directly. Finite element analysis is an alternative and better option to determine the buckling load of stiff skeleton arch bridges. In nonlinear buckling analysis, an elastic buckling analysis should be conducted in advance to obtain eigenvalues and their corresponding buckling modes. Specifically, eigenvalue coefficients can be used for estimating the critical load in nonlinear buckling analysis; buckling modes can be used to determine the initial defects and the monitoring points in nonlinear buckling analysis. When conducting nonlinear buckling analysis by ANSYS, geometric nonlinearity is realised by activating the large deformation option 'NlGeom', and material nonlinearity is realized by defining the nonlinear constitutive model of relevant materials. Specifically, Hognestad model is used as the compression constitutive model of concrete (1), and the a quad-linear model is chosen as the constitutive model of steel (2), which are shown in Equations (2) and (3), respectively.

$$\begin{cases} \sigma_c = kf_{cu,k}\left[\dfrac{2\varepsilon}{\varepsilon_0} - \left(\dfrac{\varepsilon}{\varepsilon_0}\right)^2\right], 0 \le \varepsilon \le \varepsilon_0 \\ \sigma_c = f_{cu,k}\left[1 - 0.15\left(\dfrac{\varepsilon - \varepsilon_0}{\varepsilon_u - \varepsilon_0}\right)\right], \varepsilon > \varepsilon_0 \end{cases}, \tag{2}$$

where σ_c and ε are stress and strain of concrete, respectively; ε_0 is the peak strain, and is typically set to 0.002; k is a constant and is typically set to 0.833 and 0.875, for C60 and C80 concrete, respectively; $f_{cu,k}$ is the cube compressive strength of concrete.

$$\begin{cases} \sigma = E_y\varepsilon, & 0 \leqslant \varepsilon \leqslant \varepsilon_0 \\ \sigma = f_y, & \varepsilon_0 < \varepsilon \leqslant \varepsilon_1 \\ \sigma = f_y + \dfrac{E_y}{\left[150\left(\varepsilon - \varepsilon_1\right)\right]}, & \varepsilon_1 < \varepsilon \leqslant \varepsilon_2 \\ \sigma = f_u, & \varepsilon \geqslant \varepsilon_2 \end{cases}, \tag{3}$$

where E_y is the elastic modulus of steel in the elastic stage; ε_0 is the elastic limit strain; $\varepsilon_1 = 10\varepsilon_0$ represents the yield limit strain of concrete; $\varepsilon_2 = 100\varepsilon_0$ represents the strengthening ultimate strain of concrete; and f_y is the yield strength of steel; the value of steel ultimate strength $f_u = 1.6f_y$.

In nonlinear buckling analysis, external load is simplified into several step increments, and the structural stiffness under each step load remains constant when iteratively calculating the structural response by the arc length method (Li and Peng, 2022). It adopted that the imperfection amplitude is $L/5000$. Flowcharts of nonlinear buckling analysis are shown in Figure 3.

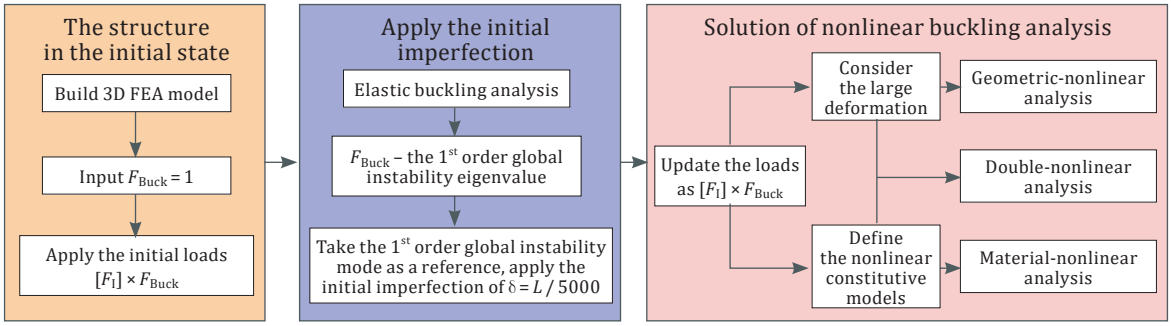

Figure 3. Flowchart of nonlinear buckling analysis

Yang (1998) studied the nonlinear buckling behaviour of a CFST arch with a span of 6.0 m in a scale model test. The arch axis of the model is a catenary with a coefficient m (arch-axis coefficient) = 1.167; the rise height f = 1.5 m. The arch ribs are made of ∅ 82 mm × 4 mm steel tubes and filled with C40 concrete. The width-span ratio is 1/40 at the vault, and is 1/20 at the arch foot. Five transverse braces are arranged uniformly along arch ribs and constructed by ∅ 60 mm × 4 mm steel tubes. The loading scheme is to simultaneously apply five concentrated loads of P and $0.03P$ in vertical and horizontal directions on the five division points. In the finite element model of this paper, BEAM188 elements are used to simulate the chord, web member, braced plane frame, and transverse brace in the stiff skeleton. The double-element method is used to simulate the cooperative behaviour of CFST. SHELL181 elements are used to simulate the surrounding concrete of arch ribs and transverse braces. The surrounding concrete is meshed by quadrilateral mapping grids with a size of 0.5 m. All translational and rotational freedom degrees of the arch foot and embedded parts are constrained. The birth and death element method in ANSYS is used to simulate the construction process of filling concrete into steel tubes and wrapping the surrounding concrete on a stiff skeleton. The load-horizontal displacement curves at the middle span and 1/3 span-wise point calculated in this paper are compared with the test results in (Yang, 1998), as shown in Figure 4. The ultimate load obtained in this paper is P = 153.4 kN, which is 94.1% of the experimental result P = 163.0 kN.

Overall, the load-deflection response obtained by FEM accords well with the test results in (Yang, 1998), the stability ultimate bearing capacity of the double-ribbed arch bridge can be evaluated conservatively by the proposed FEM method in this study. The deviation is mainly attributed to the discrepancy of boundary conditions in model test and FE analysis. First, experimental data and finite element analysis data may involve different assumptions and boundary conditions. Finite element analysis is based on a series of ideal boundary conditions, which may not fully

align with the actual conditions in the experiment, leading to errors. Second, finite element analysis often relies on idealized models of materials, while the properties of actual materials can be affected by various factors such as temperature, humidity, fatigue, etc., which may result in differences between the experimental and analysis data.

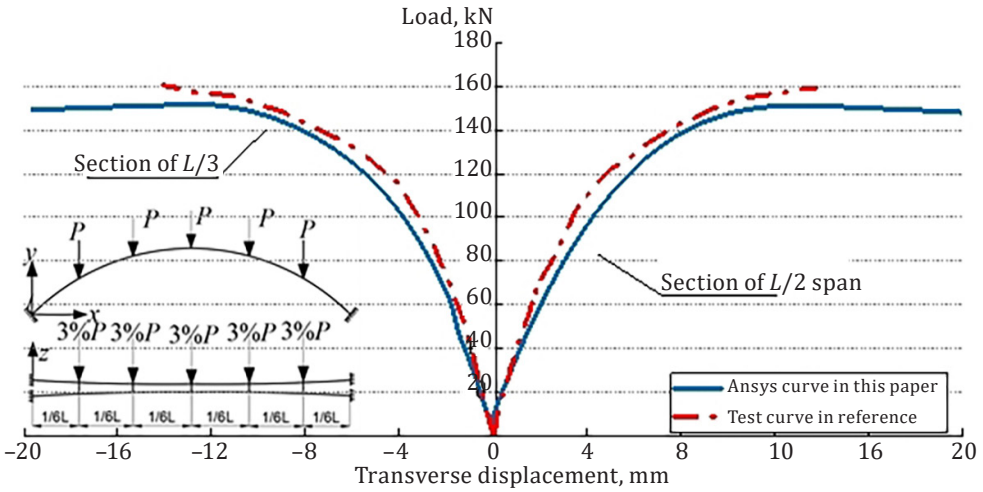

Figure 4. Load-displacement curve of the double-rib arch

1.2. A simplified method to qualitatively evaluate the extreme buckling capacity by an elastic stability coefficient

Although the proposed nonlinear analysis method by ANSYS can provide accurate ultimate buckling capacity, it is time-consuming, laborious and insufficient. Therefore, it is desired to seek for a simplified method to qualitatively evaluate the buckling performance of arch ribs during casting surrounding concrete. In that case, the pouring procedures of surrounding concrete can be optimised conveniently. As the buckling eigenvalue is proportional to structure's ultimate stability capacity, the double-nonlinear stability safety coefficient K can be represented by

$$K = \frac{\xi P_{\mathrm{Ecr}}}{P_{\mathrm{I}}} = \xi\lambda, \tag{4}$$

where P_{Ecr} is the critical buckling load corresponding to elastic instability of the arch; P_{I} is the initial load; λ is the elastic stability coefficient; ξ is the reduction coefficient after considering geometry and material nonlinearity, which is less than 1.0.

If the self-weight of concrete to be poured in the next step is GH, let $x = GH/P_1$, the self-weight of arch ribs increases by x times. Thus, the nonlinear buckling capacity of arch ribs can be assumed to be reduced by ηx times, according to the Updated Lagrangian Formulation in nonlinear analysis theory. Therefore, the double-nonlinear stability safety coefficient K' after pouring a new segment of concrete can be represented by

$$K' = \frac{\xi(1-\eta x)P'_{\mathrm{Ecr}}}{(1+x)P_1} = \xi(1-\eta x)\lambda', \tag{5}$$

where η denotes the reduction of ξ after pouring new surrounding concrete, and λ' is the elastic stability coefficient after pouring new surrounding concrete.

To ensure that the stability performance of arch ribs will not decrease after pouring new surrounding concrete, K' must be greater than K. Substituting it into Equation (4) ~ (5), yields

$$K' > K \Leftrightarrow \xi(1-\eta x)\lambda' > \xi\lambda \Leftrightarrow \frac{\lambda'-\lambda}{\eta\lambda'} > x. \tag{6}$$

The stiffness and self-weight of the arch will simultaneously increase after pouring new surrounding concrete. If the increment in stiffness surpasses self-weight, η is less than 1.0; while η is greater than 1.0 in the other condition. As arch's cross sections of stiff skeleton arch bridges are always thin-walled box section, the concrete is always cast in the place away from the centre of cross section. Consequently, the increment of area moment of inertia of arch's cross section always faster than that of the sectional area, which means that the increment in stiffness surpasses self-weight. Therefore, η is always no greater than 1.0. Conservatively, η can be set to 1.0, i.e., the double-nonlinear stability coefficient will reduce by x times after pouring the surrounding concrete in weight of x times the initial load.

Let $\varepsilon = (\lambda'-\lambda)/\lambda'$, ε is a necessary condition to prevent the buckling of arch rib after pouring new surrounding concrete. In other words, the stability capacity of arch ribs will not descend when pouring surrounding concrete.

Taking the model arch (3) as an example, a concrete transverse brace with trapezoidal plate is cast to evaluate its enhancement to the stability of arch ribs. The concrete plate is 40 mm in depth, 0.2 m in length, and with a width consistent with the spacing between two separated arch ribs. Three different pouring schemes have been analysed to seek out the optimal casting scheme, as shown in Figure 5.

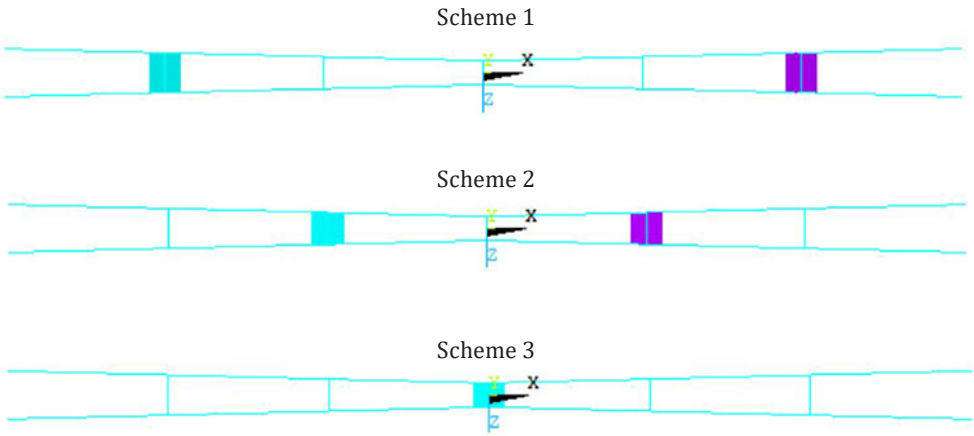

Figure 5. Cast-in-place scheme of wrapped concrete on transverse bracing (Plan view)

The initial load in self-weight direction is set to structural self-weight $G = 2566.4$ N, and the initial lateral load is set to 0.03 G. After conducting the nonlinear buckling analysis and eigenvalue analysis by ANSYS, the double-nonlinear and elastic stability coefficients can be determined. The nonlinear and elastic buckling coefficients for the stiff skeleton arch are $K = 234.4$ and $\lambda = 783.8$, respectively; while the corresponding coefficients related to the three casting schemes are listed in Table 1. The qualitative evaluation results are consistent with the nonlinear analysis results. It can be concluded that the proposed simplified method can evaluate the buckling performance of arch ribs during casting surrounding concrete accurately and efficiently.

Table 1. Calculation results for different concrete casting scheme on transverse brace

Wrapping scheme	GH	$x=GH/P_1$	λ'	$\varepsilon=(\lambda'-\lambda)/\lambda'$	Qualitative evaluation results	Nonlinear analysis results K'
Scheme 1	120.1	4.68%	859.0	8.75%	$K'>K$	238.5($>K$ = 234.4)
Scheme 2	84.2	3.28%	769.6	–1.85%	$K'<K$	226.4($<K$ = 234.4)
Scheme 3	38.0	1.48%	794.6	1.36%	$K'<K$	231.0($<K$ = 234.4)

2. Matching wrapping procedures of surrounding concrete around transverse brace and stiff skeleton

2.1. Engineering case

A stiff skeleton concrete arch bridge with a span length of 600 m is taken as an example; the rise height f = 120 m; the rise-span ratio f/L = 1/5. The arch axis is a catenary with a coefficient m = 1.6. The double-rib arch comprises two parallel concrete arch ribs with variable box-section, as shown in Figure 6. The box section at the arch foot is 12 m × 6.5 m, and the vault section is 8 m × 6.5 m. The horizontal space of the two arch ribs is 16.5 m, which are connected together by 15 concrete transverse braces reinforced by a stiff skeleton. There are two types of transverse braces, i.e., the transverse brace with a single truss piece (Figure 7) and the transverse brace in the form of a truss structure (Figure 8). The transverse braces in the truss structure comprise paired truss elements connected by an M-shaped frame. They are strategically positioned at the spandrel columns, with additional single-truss transverse braces installed between these columns. For clarity and easy reference, we have numbered the braces sequentially along the span-wise direction of the arch ribs, as shown in Figure 9, in which DH represents single-truss transverse braces, and SH represents truss-structural transverse braces. This numbering system facilitates a clear distinction between the two types of braces, enhancing understanding of their positioning and roles in the overall structure.

a) Overall arrangement of a reinforced concrete bridge with stiffened skeleton (unit: m)

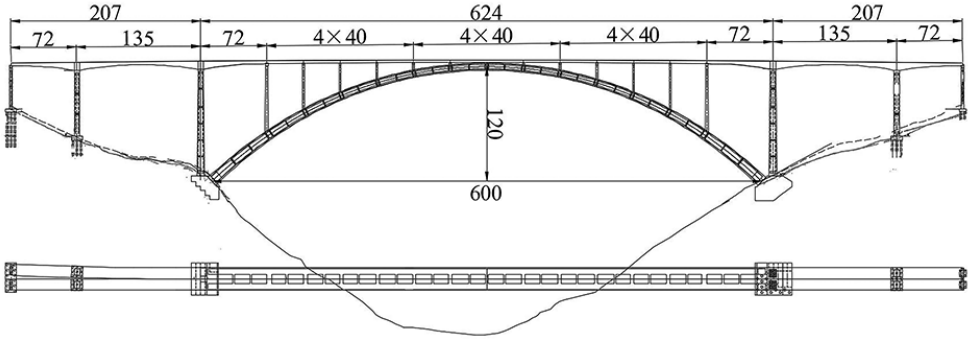

b) Cross-section of the arch vault and spring (unit: mm)

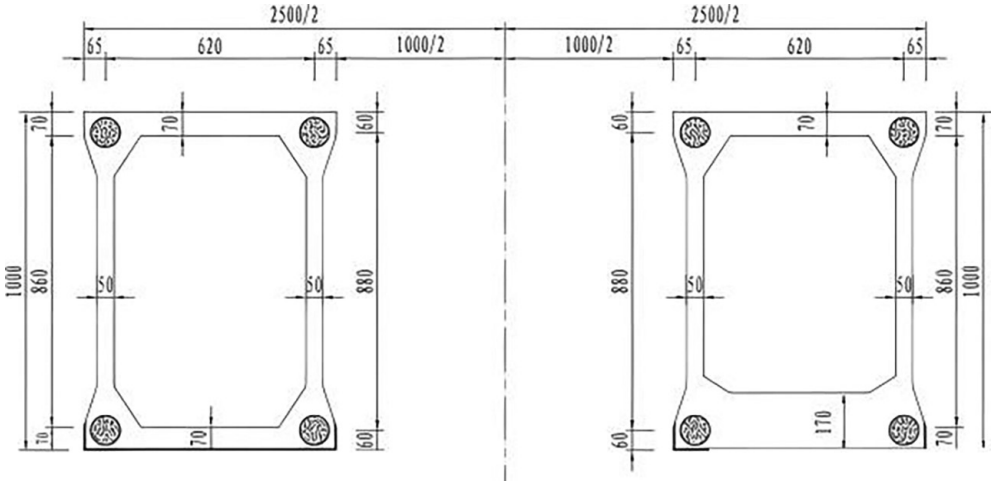

Figure 6. Three views of the arch

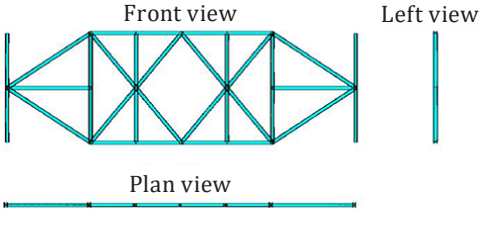

Figure 7. Three views of a transverse brace with a single truss piece

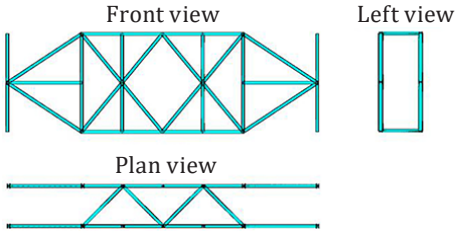

Figure 8. Three views of a truss-structural transverse brace

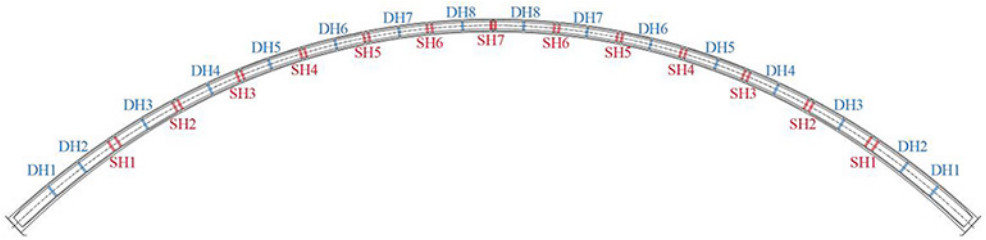

Figure 9. Numbering of all transverse braces of arch ribs

A FE model of this double-rib arch has been established to analyse its stability performance when wrapping the surrounding concrete, as shown in Figure 10. The global coordinate system of the FE model is defined with the X-axis representing the longitudinal direction, the Y-axis representing the vertical direction, and the Z-axis representing the lateral direction. BEAM188 elements are used to simulate the chord, web member, braced plane frame, and transverse brace in the stiff skeleton. The double-element method is used to simulate the cooperative behaviour of CFST. SHELL181 elements are used to simulate the surrounding concrete of arch ribs and transverse braces. The surrounding concrete is meshed by quadrilateral mapping grids with a size of 0.5 m. Specifically, we conducted a series of simulations with varying mesh densities to assess the convergence of the results. The assumed dimension of the FE was set at 0.5, which was chosen based on preliminary studies and expert recommendations. To verify this dimension, we compared the results obtained with different mesh sizes, ranging from 0.25 to 1.0. The results showed that as the mesh size decreased from 1.0 to 0.5, the numerical solutions converged to a stable value, indicating that the chosen dimension of 0.5 was appropriate for achieving accurate and reliable results. In summary, the FE convergence analysis confirmed that the assumed dimension of 0.5 was verified and suitable for the simulations conducted in this study. This ensures that the numerical results are accurate and can be used for further analysis and conclusions. A mesh size that is too small will affect computing efficiency. All translational and rotational freedom degrees of the arch foot and embedded parts are constrained. The birth and death element method in ANSYS is used to simulate the construction process of filling concrete into steel tubes and wrapping the surrounding concrete on a stiff skeleton.

The following parameters are used in the calculation of FEs:

1. Element Formulations. BEAM188: Based on Timoshenko beam theory (accounting for shear deformation), employing quadratic displacement shape functions (second-order interpolation along length) with full integration (2 Gauss points) to ensure elastic stress accuracy. SHELL181: Based on Mindlin-Reissner shell theory (including transverse shear), adopting bilinear shape

functions (first-order in-plane interpolation) with full-order integration (2×2 Gauss points).

2. DOF and Special Effects. Both elements activated 6 DOFs (UX/UY/UZ/ROTX/ROTY/ROTZ). BEAM188: Warping DOF disabled (default, neglecting section distortion). SHELL181: Thick-shell formulation enabled (3 Simpson points through thickness).
3. Nonlinear Controls. Geometric nonlinearity: large deformation effects activated (NLGEOM, ON). Material nonlinearity: Steel with bilinear kinematic hardening; concrete with William-Warnke five-parameter criterion. Solver: Arc-length method (ARCLEN) for buckling analysis; convergence tolerance: energy norm (TOLER = 0.5%).
4. Validation Basis. Mesh sensitivity analysis confirmed that at element sizes ≤ $L/15$ (L – member length), eigenvalue buckling load errors remained <2%, satisfying engineering accuracy (verified against Timoshenko's classical solution).

The material characteristics used in the model are shown in Table 2.

a) Three views of stiffened skeleton

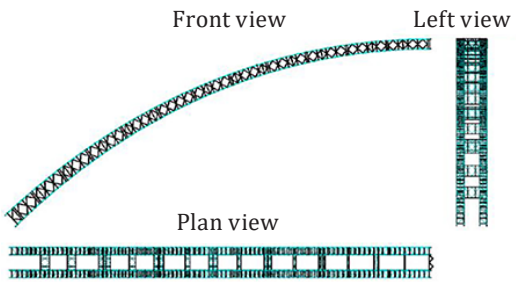

b) The entire arch ribs after wrapping the surrounding concrete

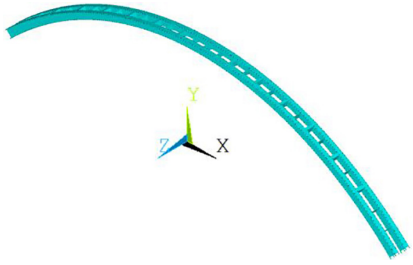

Figure 10. Finite element model of arch ribs

Table 2. Material parameters in the finite element model

Component	Material type	Yield point, MPa	Elastic modulus, GPa	Shear modulus, GPa	Density, kN/m^3	Possion's ratio
Chord of arch ribs	Q420D	420	210	80.2	78.5	0.31
Core concrete	C80		38	15.8	26	0.2
Web member of arch ribs, transverse bracing	Q335C	335	206	78.6	78.5	0.31
Surrounding concrete	C60		36	15.0	26	0.2

According to the Hognestad model of concrete and the quad-linear model of steel, the multi-linear isotropic hardening (MISO) model in ANSYS is used to simulate the constitutive model of concrete and steel, as shown in Figure 11.

a) concrete **b)** steel

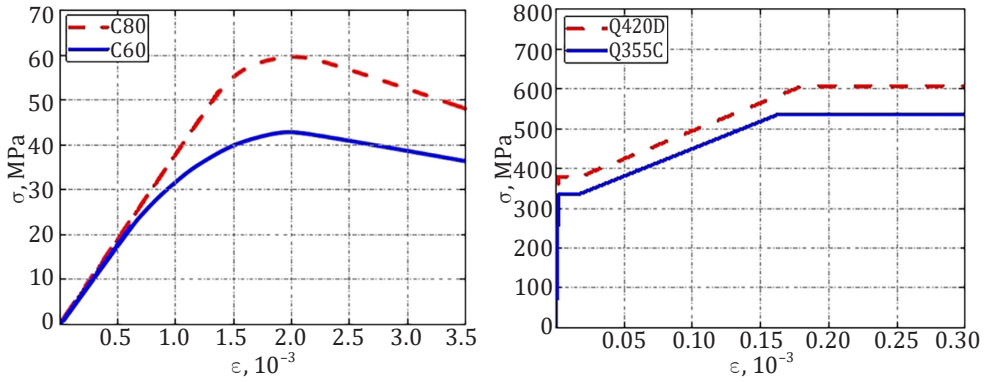

Figure 11. Constitutive models of materials

Elastic buckling analysis and double-nonlinear buckling analysis are conducted for the double-rib stiff skeleton arch without concrete pouring. The first out-of-plane buckling mode is shown in Figure 12a. The out-of-plane elastic stability coefficient is 3.39, and the nonlinear stability coefficient is 3.14, which is 7.4% less than the elastic stability coefficient, indicating that the material stress is at a low level when buckling occurs, and that the nonlinearity is mainly manifested as geometric nonlinearity. Besides, it can also be observed that large lateral deflection occurs when arch ribs buckle.

a) deformation shape of the first buckling mode

b) deflection angles of arch ribs at the critical state of bulking

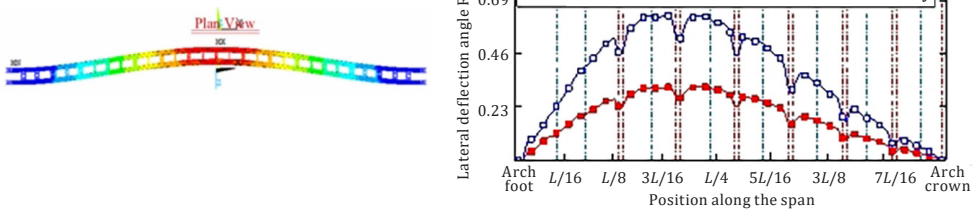

Figure 12. Deflection of the stiffness skeleton under buckling load

It is important to highlight that in large-span stiff skeleton concrete arch bridges, the out-of-plane stiffness is observed to be less than the in-plane stiffness, due to the limited sectional stiffness of arch ribs and the large-spaced arrangement of transverse braces. The lateral deflection around the Y axis is referred to as the lateral deflection angle in this paper. The lateral deflection angle of the double-rib stiff skeleton arch under the buckling load is plotted in Figure 12b, in which the dash-dot lines coloured blue correspond to the locations of transverse braces with a single truss piece, dash-dot lines coloured red correspond to the locations of the truss-structural transverse braces. It is evident that the lateral deflection angle of arch ribs exhibits a gradual transition at the positions of transverse braces with a single truss piece, whereas a sudden decrease occurs at the locations of truss-structural transverse braces. This phenomenon suggests that transverse braces with a single truss piece inadequately constrain the rotational angle of two isolated arch ribs during lateral bending, primarily due to their limited bending stiffness along the tangential direction of the arch. The M-shaped horizontal frames integrate the two truss pieces of transverse brace into a cohesive truss structure, significantly augmenting the stiffness of transverse braces along the tangential direction of arch ribs. Therefore, the truss-structural transverse braces are capable of constraining the lateral deflection angle of arch ribs. In addition, the lateral deflection angle of arch ribs reaches its peak value in the range of L/8 span-wise point to 3L/8 span-wise point. Therefore, it can be concluded that placing several truss-structural transverse braces in the range of L/8 span-wise point to 3L/8 span-wise point may achieve the most effective control effect for lateral deflection angle, which also explains why researches (4–7) conclude that the arrangement of transverse braces between arch foot and quarter-point of arch has the best improvement effect on the out-of-plane stability of arch ribs, while the effect of arrangement in the vault is not apparent.

Therefore, the mechanism of transverse braces enhancing the lateral bending stiffness of arch ribs can be summarised as follows: the transverse brace between separated arch ribs relies on its strong tangential stiffness along arch axis to coordinate the lateral bending deformation of two separated arch ribs, to reduce the lateral deflection angle and to improve the out-of-plane bending stiffness of double-rib arch. (8) also pointed out that initiating the pouring of transverse support concrete at the L/4 position maximises the stability and load-bearing capacity of bare arch. Hence, in the subsequent optimisation of the pouring procedure for transverse brace concrete, the process begins with concrete pouring at the L/4 transverse brace.

Considering the pronounced impact of the flexural stiffness of the transverse brace between ribs on the stability of arch ribs, it is noteworthy that the out-of-plane stiffness of the double-rib arch is smaller than its in-plane stiffness. It can be seen from Table 3 that when pouring the surrounding concrete around SH1~ SH4

(L/8 ~ 3L/8), the overall lateral deflection angle of the arch reduces. Significantly, after pouring the concrete on SH3 at L/4, the out-of-plane rotation angle of arch ribs close to both ends of the transverse brace decreases uniformly, thus the corresponding out-of-plane stability coefficient reaches the highest.

Table 3. Out-of-plane instability coefficient when casting the wrapping concrete on a truss-structure transverse brace and its corresponding δ_z

Pouring condition	None	SH1	SH2	SH3	SH4	SH5	SH6	SH7
Elastic stability coefficient	3.39	3.5	3.55	3.66	3.56	3.27	3	3.12
δ_z, m	0.307	0.304	0.303	0.286	0.285	0.312	0.346	0.334

2.2. Optimization method and result for casting procedures of the surrounding concrete on the transverse brace

The pouring of transverse brace concrete near L/4 demonstrates optimal control over the out-of-plane deflection angle of double-rib arch. Symmetrical concrete pouring around the transverse brace from the L/4 point to both sides significantly enhances the stability of double-rib arch, which is adopted in the following optimization. The recommended pouring scheme can be ascertained by following the procedural steps outlined in Figure 13. The initial structural loads are updated in accordance with the already determined location of the transverse brace concrete to be poured before the bottom slab concrete.

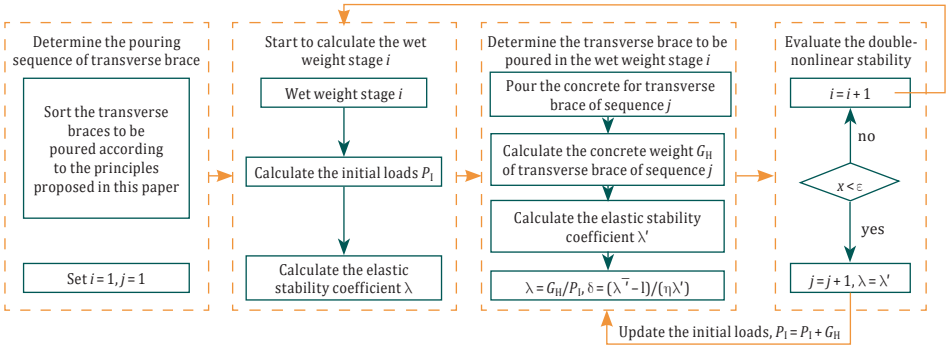

Figure 13. Optimisation method for the pouring procedure of the surrounding concrete of the transverse brace

According to Figure 13, the initial pouring procedure of the transverse brace can be set to: (1)SH6→(2)SH7&SH5→(3)SH8&SH4→(4)SH9&SH3→(5)SH2&SH10→(6)SH1&SH11→(7)SH12, and the optimisation results of the concrete pouring scheme in each wet weight stage are summarised in Tables 4–7.

Table 4. Optimisation procedure for concrete pouring around transverse brace in the wet weight stage of the bottom slab

Poured brace number	Elastic stability coefficient	Initial load (106 N)	Self-weight (106 N)	*x*	ε
None	2.24	272.2	–	–	–
SH6	2.35	272.2	12.2	4.50%	4.68%
x<ε, calculate the results of the next pouring brace on this basis					
SH5, SH7	2.43	284.4	24.6	8.65%	1.65%
x>ε, stop					

Table 5. Optimisation procedure for concrete pouring around transverse brace in the wet weight stage of the lower half web

Poured brace number	Elastic stability coefficient	Initial load (106 N)	Self-weight (106 N)	*x*	ε
SH6	2.56	417.8	–	–	–
SH5, SH7	2.79	417.8	24.6	5.89%	8.24%
x>ε, calculate the results of the next pouring brace on this basis					
SH4, SH8	2.99	442.4	24.6	5.56%	6.69%
x>ε, calculate the results of the next pouring brace on this basis					
SH3, SH9	3.21	467.0	25.0	5.35%	6.85%
x>ε, calculate the results of the next pouring brace on this basis					
SH2, SH10	3.33	492.0	25.3	5.14%	3.60%
x>ε, stop					

Table 6. Optimisation procedure for concrete pouring around transverse brace in the wet weight stage of the upper half web

Poured brace number	Elastic stability coefficient	Initial load (106 N)	Self-weight (106 N)	*x*	ε
SH3~SH9	3.62	627.3	–	–	–
SH2, SH10	3.89	627.3	25.3	4.03%	6.94%
x<ε, calculate the results of the next pouring brace on this basis					
SH1, SH11	4.0 (in-plane)	652.6	25.4	3.89%	2.75%
x>ε, stop					

Table 7. Optimisation procedure for concrete pouring around transverse brace in the wet weight stage of the roof plate

Poured brace number	Elastic stability coefficient	Initial load (106 N)	Self-weight (106 N)	x	ε
SH2~SH10	4.22	779.1	–	–	–
SH1, SH11	4.40	779.1	25.4	3.26%	4.09%
$x<\varepsilon$, calculate the results of the next pouring brace on this basis					
SH12 (arch crown)	4.32	804.5	7.2	0.9%	–1.85%
$x>\varepsilon$, stop					

Based on the optimisation results presented above, the optimal procedure for wrapping the surrounding concrete on stiff skeleton arch ribs and transverse brace is as follows.

(1) Before pouring the concrete of the arch rib's bottom plate, wrap the surrounding concrete on SH6.
(2) After the closure of the bottom plate, wrap the surrounding concrete on SH5 and SH7 first, then SH4 and SH8, then SH3 and SH9, and finally pour the lower half web concrete.
(3) After the closure of the lower half web, wrap the surrounding concrete on SH2 and SH10, then pour the upper half web concrete.
(4) After the closure of the upper half web, wrap the surrounding concrete on SH1 and SH11, then pour the top plate concrete.
(5) After the closure of the top plate, wrap the surrounding concrete on SH12.

3. Mechanism of the transverse brace to enhance the out-of-plane buckling capacity of the double-rib arch

The process of wrapping surrounding concrete around arch ribs without accounting for the pouring procedure of transverse brace concrete is denoted as the pre-control construction process. In contrast, the optimised matching wrapping procedure of surrounding concrete is referred to as the post-control construction process. Nonlinear buckling analysis was conducted to calculate the stability capacity corresponding to each wet weight condition during the concrete wrapping process. Table 8 shows the stability safety factors calculated by different analysis methods. The percentage within brackets denotes the stability factor calculated through nonlinear analysis relative to the results obtained from eigenvalue analysis.

It can be seen from Table 8 that the double-nonlinear stability coefficients of the double-rib arch in the wet weight stage before control do not meet the requirements in specification (9), which requires the nonlinear stability coefficient to be at least 1.75. However, the double-nonlinear stability coefficient after control is more significant than 1.75 in each wet weight stage. The double-nonlinear stability coefficient in the wet weight stage when pouring top-plate concrete increases by 22.9% compared to the results before control.

Due to the fact that the actual structure is bound to be affected by dual nonlinearity, the stability optimisation of this bridge in this paper is sufficient to ensure the safety of the concrete external wrapping process of the main arch. Moreover, as described in the code, for stiff skeleton arch bridges, merely meeting the elastic stability requirements is not enough to guarantee the safety of the structure.

Table 8. Instability coefficient of arch ribs at different construction states

Wet weight stage		Eigenvalue	Only geometric nonlinearity	Only material nonlinearity	Double-nonlinearity
Before control	Bottom plate	1.82(100%)	1.74(95.6%)	–	1.70(93.4%)
	Lower half web	1.84(100%)	1.77(96.2%)	–	1.66(90.2%)
	Upper half web	1.85(100%)	1.75(94.5%)	–	1.66(89.7%)
After control	Bottom plate	2.35(100%)	2.12(90.2%)	–	2.05(87.2%)
	Lower half web	3.21(100%)	3.09(96.3%)	2.32(72.3%)	1.87(58.3%)
	Upper half web	3.89(100%)	3.64(93.6%)	2.58(66.3%)	2.04(52.4%)

Figure 14 illustrates the load-displacement curves for each wet weight stage before and after control. Evidently, pouring surrounding concrete around the transverse brace significantly enhances the overall lateral bending stiffness of arch ribs, effectively restricting their lateral deformation. Furthermore, Figure 14 indicates that when the lateral bending stiffness of arch ribs is low, geometric nonlinearity predominates as the primary nonlinearity factor; conversely, when the lateral bending stiffness is high, material nonlinearity becomes the dominant factor. The coupled effect of geometric and material nonlinearity consistently diminishes the stability capacity of arch ribs.

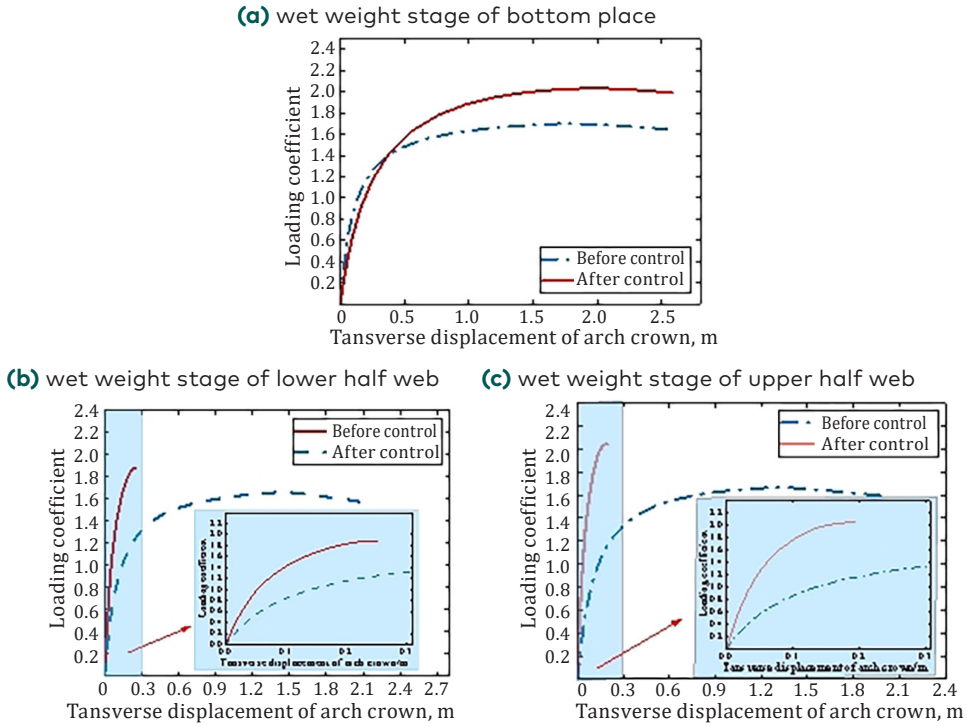

Figure 14. Load-displacement curves at the middle span of arch ribs corresponding to different construction stages

Figure 15 shows the Von-Mises stress distribution in the arch ribs at the critical buckling state corresponding to the lower half web's weight stage. Certain intersection regions between the transverse brace's chord and the arch rib's chord initially yield, and then these yielding areas extend throughout the entire cross-section. Consequently, it can be concluded that these intersection regions create plastic hinges, significantly compromising the lateral bending stiffness of the main arch. When the plastic hinge count reaches a specific threshold, the lateral stiffness becomes inadequate to withstand any lateral loads, resulting in the buckling of arch ribs.

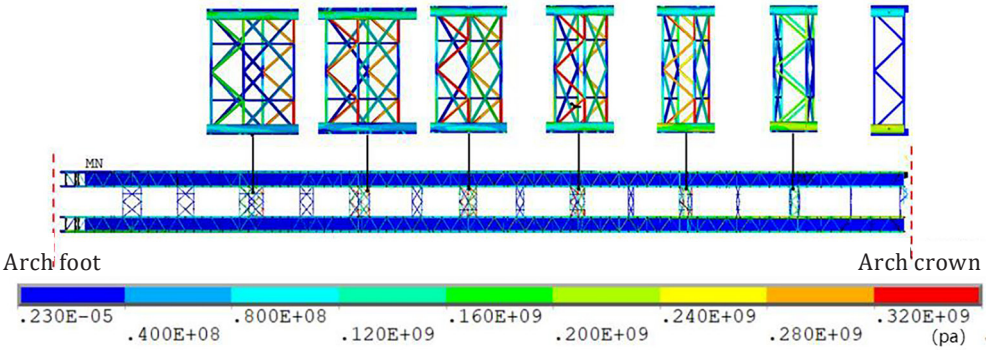

Figure 15. Von-Mises stress diagram of the arch ribs at the critical state of buckling corresponding to the wet weight stage of lower half web without control

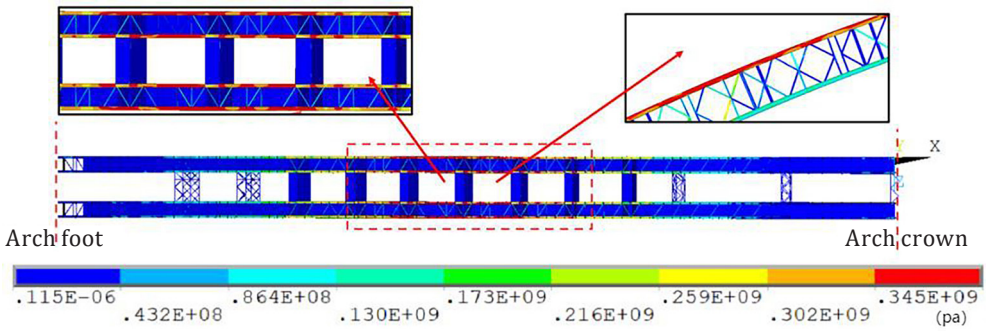

Figure 16. The Von-Mises stress diagram of arch ribs at the critical state of buckling corresponding to the wet weight stage of the lower half web after control

Figure 16 plots Von-Mises stress distribution in arch ribs at the critical buckling state corresponding to the wet weight stage of the lower half web after control. Evidently, the absence of plastic hinges is observed after pouring of the transverse brace concrete, as the surrounding concrete on the transverse braces effectively shares the stress. However, a substantial plastic zone manifests in the chords of arch ribs near the 1/4 span-wise point. The emergence of these plastic zones diminishes the overall lateral bending stiffness of the main arch, consequently leading to significant plastic deformation. As the plastic zone expands to a critical extent, the double-rib arch becomes incapable of maintaining stable equilibrium, ultimately resulting in instability.

Apart from enhancing the buckling capacity of arch ribs, casting procedures of surrounding concrete on transverse braces may have a great potential to alleviate the stress in steel pipes and filled concrete of stiff skeletons. Table 9 compares

stress in steel pipes and filled concrete before and after control. The extreme stress exhibits a discernible improvement, demonstrating a maximum reduction of 7.1% in the peak compressive stress of steel tubes and a maximum reduction of 12.9% in the peak compressive stress of core concrete in the tubes. The post-control construction process showcases significant effectiveness.

Table 9. Comparison of stress in the steel pipes and concrete inside the pipes before and after control, MPa

Construction phase of a stiff skeleton arch bridge	Before control				After control			
	Stiff skeleton stress at 1/16 span-wise point		Stiff skeleton stress at 1/2 span-wise point		Stiff skeleton stress at 1/16 span-wise point		Stiff skeleton stress at 1/2 span-wise point	
	Upper surface	Lower surface	Upper surface	Lower surface	Upper surface	Upper surface	Upper surface	Upper surface
	Steel tube	Concrete	Steel tube	Concrete	Steel tube	Concrete	Steel tube	Concrete
The first ring formed	–185	–16.3	–179	–11.5	–185	–16.3	–179	–11.5
The second ring formed	–224	–23.3	–238	–22.3	–225	–23.5	–252	–24.8
The third ring formed	–257	–29.2	–307	–35.1	–248	–27.6	–284	–30.5
The fourth ring formed	–266	–30.9	–319	–37.2	–257	–29.3	–294	–32.6
The fifth ring formed	–282	–33.8	–336	–40.2	–275	–32.5	–310	–35.6
The sixth ring formed	–294	–36.5	–349	–42.7	–287	–34.7	–326	–38.5

Besides, Figure 17 shows that the lateral deflection angle of the main arch after control is several times lower than that without control. The lateral deformation d_z without control is 1.48 m and reduces to 0.22 m (by 83%) after control, indicating that pouring surrounding concrete on transfers brace significantly improves the lateral bending stiffness of double-rib arch.

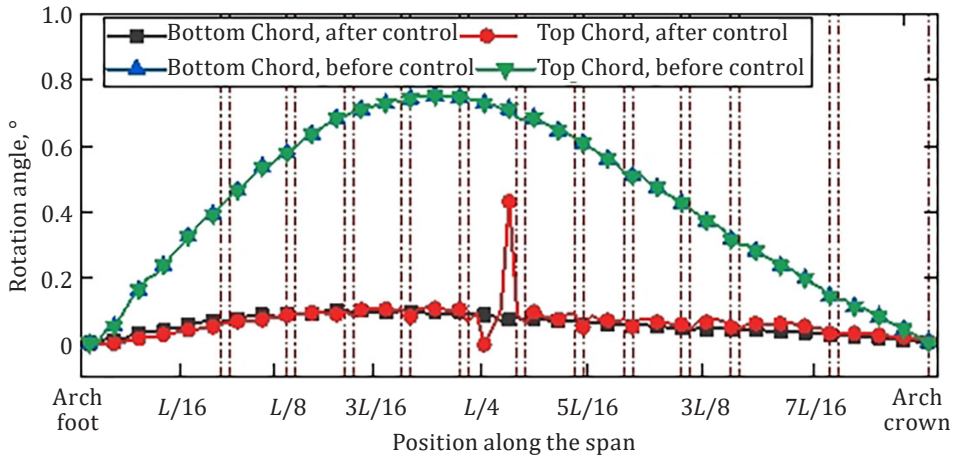

Figure 17. The rotation angle caused by lateral bending of arch ribs at the critical state of buckling corresponding to the wet weight stage of the lower half web, with and without control

Through a comparative analysis of the buckling mechanism before and after the application of surrounding concrete on the transverse brace, it can be inferred that prior to concrete wrapping, the coupling effect of geometric and material nonlinearity induced the formation of plastic hinges at the intersection point between the transverse brace's chord and the rib chord, ultimately resulting in the out-of-plane buckling of the main arch. Conversely, following the casting of surrounding concrete on the transverse brace, the coupling effect of geometric and material nonlinearity initiates the formation of a plastic zone originating from the arch rib chord at the 1/4 span-wise point, which progressively expands. The gradual expansion of these regions eventually culminates in the out-of-plane buckling of the arch ribs.

Conclusion

The paper introduces a streamlined assessment approach to qualitatively evaluate the anticipated reduction in double-nonlinear stability following the application of surrounding concrete on the transverse brace. This assessment relies on outcomes derived from an elastic stability analysis. Additionally, the investigation delves into and elucidates the mechanism through which the transverse brace augments the out-of-plane stability capacity of the double-rib arch. Building upon these insights, an optimisation methodology is proposed to ascertain

an optimal casting scheme for surrounding concrete, taking into account both the stiff skeleton and the transverse brace.

In the condition where each concrete arch ring on stiff skeletons is nearing closure, the stability scenario becomes notably challenging. Particular emphasis is warranted on assessing the stability of a double-rib stiff skeleton concrete arch bridge under such circumstances. The transverse braces assume a pivotal role in effectively coordinating and constraining the lateral bending deformation of the two isolated arch ribs. This is accomplished by leveraging their bending stiffness along the tangential direction of the arch axis. It is noteworthy that the transverse braces situated within the L/8 to 3L/8 range make the most substantial contribution to the lateral stiffness of the arch ribs.

Pre-emptive wrapping of the surrounding concrete on the transverse brace is recommended at the L/4 span-wise point prior to the closure of the bottom plate's concrete ring. Following the closure of bottom plate's concrete ring, it is advisable to symmetrically pour the wrapping concrete on the transverse brace towards the arch foot and vault from the L/4 span-wise point. This approach aims to bolster the overall stability capacity of the arch rib during the process of wrapping concrete on the stiff skeletons.

When the transverse brace lacks surrounding concrete, geometric nonlinearity significantly influences the buckling behaviour of the stiffened skeleton arch. Hence, it becomes imperative to restrict the lateral deflection of the double-rib arch during this construction stage. The development of plastic hinges further weakens the transverse brace's capacity to constrain lateral deformation, ultimately leading to the out-of-plane buckling of the double-rib arch. Conversely, upon the application of surrounding concrete on the transverse brace, material nonlinearity assumes a primary role in undermining the stability of the main arch. Plastic hinges cease to emerge during buckling, giving way to the formation of a plastic zone on the arch ribs' chord, thereby inducing out-of-plane instability. Therefore, a comprehensive assessment of the double-rib arch's stability across various construction stages necessitates a consideration of both geometric and material nonlinearity effects, along with the presence of surrounding concrete.

This study proposes a stability optimisation method for the construction of stiffened skeleton arch bridges, with the following core values: Mechanism innovation – It reveals how the encased concrete in lateral bracing transforms the instability mode from geometrically nonlinear-dominated sudden buckling to materially nonlinear-dominated progressive failure, and identifies the critical supporting role of the L/8-3L/8 span range. Construction optimisation: A phased encasement strategy is proposed – first strengthening the L/4 zone supports, followed by symmetrical pouring of the arch springing and crown – enhancing out-of-plane stability bearing capacity by 15–20% and significantly reducing closure risks. Engineering applicability: By simplifying biaxial nonlinear evaluation based

on elastic analysis, rapid decision-making is achieved, and a full-cycle stability control framework is established, advancing empirical construction toward theoretically precise regulation. This method provides critical theoretical support and practical guidance for the safe and efficient construction of long-span stiffened skeleton arch bridges.

Declaration of Conflicting Interests

The authors declare that they have no known competing financial interests or personal relationships that could have appeared to influence the work reported in this paper.

Data availability

Data will be made available on request.

REFERENCES

Chang, W. F., and Ferguson, P. M. (1963). Long-hinged reinforced concrete columns. *Journal of the American Concrete Institute*, *60*(1), 1–25.

Chen, F., He, S., Hu, D., Liu, L., and Fan, W. (2010). Nonlinear stability analysis of the CFST double X-arch bridge. *Journal of Xi'an University of Architecture & Technology (Natural Science Edition)*, *42*(5), 649–655.

Chen, S., Hou, C., Zhang, H., and Han, L. H. (2019). Structural behaviour and reliability of CFST trusses with random initial imperfections. *Thin-Walled Structures*, *143*, Article 106192. https://doi.org/10.1016/j.tws.2019.106192

Cheng, J., Jiang, J. J., Xiao, R. C., and Xiang, H. F. (2002). Ultimate behavior of long-span steel arch bridges. *Structural Engineering & Mechanics*, *14*(3), 331–343. https://doi.org/10.12989/sem.2002.14.3.331

China, M. et al. (2015). Code for design of highway concrete filled steel tube arch bridge. China Communications Publishing, Beijing.

Ding, F., Cao, Z., Lyu, F., Huang, S., Hu, M., and Lin, Q. (2022). Practical design equations of the axial compressive capacity of circular CFST stub columns based on finite element model analysis incorporating constitutive models for high-strength materials. *Case Studies in Construction Materials*, *16*, Article e01115. https://doi.org/10.1016/j.cscm.2022.e01115

Dong, R., Chen, Y., Zheng, M., Huang, F., and Chen, B. (2020). Stability analysis of long-span CFST truss arch bridges with L-shaped bracings. *Journal of Civil Engineering*, *53*(5), 89–99.

Dou, C., and Pi, Y.-L. (2016). Flexural-torsional buckling resistance design of circular arches with elastic end restraints. *Journal of Structural Engineering*, *142*(2). https://doi.org/10.1061/(ASCE)ST.1943-541X.0001373

Geng, Y., Ranzi, G., Wang, Y., and Wang, Y. (2018). Out-of-plane creep buckling analysis on slender concrete-filled steel tubular arches. *Journal of Constructional Steel Research*, *140*, 174–190. https://doi.org/10.1016/j.jcsr.2017.10.010

Godden, W. G. (1954). The lateral buckling of tied arches. *Proceedings of the institution of Civil Engineers*, *3*(4), 496–514. https://doi.org/10.1680/ipeds.1954.12584

Gu, Y. (2011). *Stability analysis of long-span concrete arch bridge with stiff skeleton*. Southwest Jiaotong University, Chengdu.

Ji, R., and Shi, M. (2011). Stability analysis of long span railway CFST tied-arch bridge. *Journal of Vibration and Shock*, *30*(8), 87–91.

Li, L., Chen, Z., and Ge, Y. (2008). Effects of arch rib crossbars on dynamic and stabilization characteristics of concrete filled steel tubular arch bridge. *Journal of Highway and Transportation Research and Development*, *3*(2), 70–74. https://doi.org/10.1061/JHTRCQ.0000253

Li, Z., and Peng, Y. (2022). The base force element method based on the arc-length method for stability analysis. *International Journal of Non-Linear Mechanics*, *144*, Article 104088. https://doi.org/10.1016/j.ijnonlinmec.2022.104088

Liu, A. R., Huang, Y. H., Yu, Q. C., and Rao, R. (2014). An analytical solution for lateral buckling critical load calculation of leaning-type arch bridge. *Mathematical Problems in Engineering*, 1–14. https://doi.org/10.1155/2014/578473

Lu, P. Z., Li, D. G., Hong, T., Chen, Y. R., and Shi, Q. T. (2022). Concrete performance time-varying effect of CFST arch bridges. *Mechanics of Time-Dependent Materials*, *26*(2), 377–395. https://doi.org/10.1007/s11043-021-09492-2

Luo, K., Pi, Y.-L., Gao, W., Bradford, M. A., and Hui, D. (2015). Investigation into long-term behaviour and stability of concrete-filled steel tubular arches. *Journal of Constructional Steel Research*, *104*, 127–136. https://doi.org/10.1016/j.jcsr.2014.10.014

Mackenzie, D., Boyle, J., and Hamilton, R. (2000). The elastic compensation method for limit and shakedown analysis: a review. *The Journal of Strain Analysis for Engineering Design*, *35*(3), 171–188. https://doi.org/10.1243/0309324001514332

Pi, Y., Bradford, M. A., and Qu, W. (2011). Long-term non-linear behaviour and buckling of shallow concrete-filled steel tubular arches. *International Journal of Non-Linear Mechanics*, *46*(9), 1155–1166. https://doi.org/10.1016/j.ijnonlinmec.2011.05.003

Rakici, S. C., and Menkulasi, F. (2021). Out-of-plane buckling strength of free standing singly symmetric hollow pinned circular arches. *Journal of Constructional Steel Research*, *186*, Article 106914. https://doi.org/10.1016/j.jcsr.2021.106914

Shao, C., Ju, J. W. W., Han, G., and Qian, Y. (2017). Seismic applicability of a long-span railway concrete upper-deck arch bridge with CFST rigid skeleton rib. *Structural Engineering & Mechanics*, *61*(5), 645–655. https://doi.org/10.12989/sem.2017.61.5.645

Song, F., and Chen, B. (2012). Analysis of out-of-plane elastic buckling of standard concrete filled steel tubular truss ribs arch. *Engineering Mechanics*, *29*(9), 125–132.

Stüssi, F. (1943). Kippen und Querschwingungen von Bogenträgern. *Int. Assoc. of Bri. and Str. Engrs. Pubs*., *7*, 327–343.

Tong, J., Lin, Z., and Zhou, Q. (2022). Local stability of concrete arch bridge based on Ritz method. *Journal of Computational Methods in Sciences & Engineering*, *22*(1), 279–294. https://doi.org/10.3233/JCM-215644

Waestlund, G. (1960). Stability problems of compressed steel members and arch bridges. *Journal of the Structural Division*, *86*(6), 47–71. https://doi.org/10.1061/JSDEAG.0000535

Wang, M., Wu, H., Qian, J., and Chao, Y. (2018). Analysis on the influence of construction procedure of transverse bracing on the structural behavior of reinforced concrete arch bridge with rigid skeleton. *Journal of China and Foreign Highway*, *3*.

Xie, K., Wang, H., Guo, X., and Zhou, J. (2021). Study on the safety of the concrete pouring process for the main truss arch structure in a long-span concrete-filled steel tube arch bridge. *Mechanics of Advanced Materials and Structures*, *28*(7), 731–740. https://doi.org/10.1080/15376494.2019.1601309

Xu, L., Yang, H., and Liu, S. (2007). Stability analysis of long-span deck-type CFST arch bridge. *Journal of Highway & Transportation Research & Development*, *2*(1), 62-65. https://ascelibrary.org/doi/pdf/10.1061/JHTRCQ.0000170

Yang, L., Yu, B., and Ju, J. W. (2015). Incorporated strength capacity technique for limit load evaluation of trusses and framed structures under constant loading. *Journal of Structural Engineering*, *141*(11), Article 04015023. https://doi.org/10.1061/(ASCE)ST.1943-541X.0001252

Yang, Y. (1998). *Study on transverse stability of concrete-filled steel tube arch bridge*. Southwest Jiaotong University, Chengdu.

Zhao, C., Duan, J., Tang, C., Deng, K., Shang, C., and Zhang, X. (2021). Seismic performance analysis of CFST stiff skeleton concrete arch bridge considering non-planar sectional stress induced by balanced ring-casting construction. *Journal of Earthquake Engineering*, *27*(1), 84–101. https://doi.org/10.1080/13632469.2021.1997837

Zheng, J. L., and Wang, J. J. (2017). Concrete-filled steel tube arch bridges in China. *Engineering*, 4(1), 143–155. https://doi.org/10.1016/j.eng.2017.12.003

Zheng, X., Zhou, Y., Qu, Q., and Wu, W. (2012). Analysis of stability and influences of temporary cross bracings of PC tied arch bridge at construction stages. *Bridge Construction*, *42*(1), 67–71.

Zheng, J. (2024). Recent construction technology innovations and practices for large-span arch bridges in China. *Engineering*, *41*(10), 110–129. https://doi.org/10.1016/j.eng.2024.05.019